Chinese Chemical Letters 31 (2020) 1717–1728

Contents lists available at ScienceDirect

Chinese Chemical Letters

journal homepage: www.elsevier.com/locate/cclet

Review

Ag_2S nanoparticles as an emerging single-component theranostic agent

Ruxia Han, Jinrong Peng, Yao Xiao, Ying Hao, Yanpeng Jia, Zhiyong Qian*

State Key Laboratory of Biotherapy and Cancer Center, West China Hospital, West China Medical School, Sichuan University, and Collaborative Innovation Center of Biotherapy, Chengdu 610041, China

ARTICLE INFO

Article history:
Received 3 February 2020
Received in revised form 12 March 2020
Accepted 13 March 2020
Available online 16 March 2020

Keywords:
Ag_2S nanoparticle
Different sizes
Photothermal effect
Fluorescence characteristics
Theranostics

ABSTRACT

Last two decades, with the rapid changes and development of nanotechnology and biological materials, diverse multi-functional nanomaterials emerging, which offers a novel way to treat and diagnose diseases, and therefore spawned the new biomedical technology of theranostics, which integrates the treatment and diagnosis or monitoring of diseases into one. Ag_2S as a bio-nanomaterial with low biotoxicity has attracted more and more attention due to its good photoluminescence properties and fluorescence imaging of small animals in the second near-infrared region (NIR-II). Meanwhile, Ag_2S has the ability to absorb near-infrared light strongly because of its local surface plasma resonance (LSPR) effect and had become a kind of photothermal converters with good photothermal conversion efficiency. More interestingly, both photothermal effect and fluorescence characteristics of Ag_2S nanoparticles (NPs) are closely related to their particle sizes. However, the relationship between photothermal effect and fluorescence characteristics of Ag_2S NPs and their sizes has not been reviewed so far. Herein, the synthesis methods and influencing factors of synthesize Ag_2S NPs with different sizes were compared firstly, and then the photothermal effect and fluorescence characteristics of Ag_2S NPs with different sizes were summarized. Finally, the possibilities and challenges of using Ag_2S NPs to construct theranostic agent were discussed in the end.

1. Introduction

Since John Funkhouser first proposed the concept of "theranostic" in 1998, this technology has attracted extensive attention in the field of nano-bio materials at home and abroad, providing a new treatment strategy for personalized medicine and precision medicine [1–4]. The integration of diagnosis and treatment of cancer has shown great potential in real-time observation of the accumulation and therapeutic effect feedback of nanometer drugs. The core technology of theranostic is the rational design of therapeutic diagnostic agents. Common therapeutic diagnostic agents mainly include multi-component therapeutic diagnostic agents and single-component therapeutic diagnostic agents. The former needs to combinate therapeutic agents and diagnostic agents on the same carrier particle [5–7]. Complex synthesis process, limited loading, leakage problem and effective release of therapeutic agents at the tumor site are the main challenges, which multi-component theranostics facing [8–10]. Meanwhile, the theranostic with multiple components will also increase the adverse effects on the human body and expand the production cost, so it is encouraged to use fewer components or a single component for simple and effective therapeutic diagnostic design [11,12].

Due to the strong and tunable characteristics of local surface plasma resonance (LSPR), photothermal nanomaterials can convert the near-infrared (NIR) light (650–1000 nm) absorbed into resonant and transferred heat energy, raising the temperature of surrounding tissues, and achieving the local killing effect [13,14]. At the same time, when these materials absorbing near-infrared light and generating thermal energy, they can also send out photoacoustic signals in the form of ultrasonic waves and pressure waves to perform photoacoustic imaging, to realize the integration of treatment and diagnosis [15–18]. At present, common photothermal nanomaterials mainly include gold nanomaterials [19,20], carbon-based nanomaterials [21–23], chalcogenide nanoparticles [24–26], organic nanomaterials [27–30] and other particles [31–34]. Therefore, the photothermal nanomaterials mentioned above can be given priority in the design of single-component therapeutic diagnostics.

Photothermal nanomaterials can be directly used to construct theranostic agents. But single-mode imaging is not accurate enough and is susceptible to tissue penetration depth and spatial

* Corresponding author.
E-mail addresses: anderson-qian@163.com, zhiyongqian@scu.edu.cn (Z. Qian).

https://doi.org/10.1016/j.cclet.2020.03.038
1001-8417/

resolution compared with bimodal or multimodal imaging, which are more advantageous in disease diagnosis, real-time observing of drug enrichment and release at targeted sites [35–38]. Fortunately, most of the above-mentioned photothermal materials have other imaging capabilities on account of their unique optical characteristics. For instance, gold nanomaterials can perform CT imaging and magnetic nanoparticles can perform MRI imaging, respectively [7,10,39]. However, CT imaging has dangerous ionizing radiation [40], soft tissue contrast is poor, spatial resolution is limited; MRI imaging signal intensity is poor, low sensitivity. At the same time, the acquisition and post-processing time of the two is longer [41–43]. In contrast, near-infrared (NIR) fluorescence imaging, especially fluorescence imaging in the second infrared region (NIR-II), is a very powerful diagnostic candidate on account of its deeper tissue penetration, higher spatial resolution, and smaller autofluorescence effects [44–47]. Nevertheless, the fluorescence quantum yield (QY) of carbon-based materials is fairly low, and the fluorescence brightness of organic small molecule dyes needs to be further improved. Therefore, sulfur quantum dots (QDs), a new class of second near-infrared (NIR-II) fluorescent nanomaterials, are receiving more and more attention and research due to their higher quantum yield and better fluorescence signal intensity [48–53]. Compared with traditional fluorescent imaging agents, they have the following advantages: 1) deeper tissue penetration and higher imaging resolution; 2) less autofluorescence, lower tissue scattering and higher signal-to-noise ratio; 3) good light stability, strong photobleaching resistance and long fluorescence lifetime [54–58]. However, the common quantum dots, such as CdS, PbS, PbSe and HgS, have been limited their medical applications due to their high toxic ions [59–61]. In contrast, Ag_2S quantum dots without hazardous ions are better choice of diagnostics in theranostics because of their advantages of better biosafety [62–64].

It has been reported that the PA signal of Ag_2S nanoparticles (NPs) in tumors is enhanced by 2.4 times (24 h after injection) for their ideal photothermal effect and better tumor targeting [65,66]. At the same time, Ag_2S NPs has a good fluorescence quantum yield, so they can provide ultrasensitive and visualized NIR-II fluorescence imaging for tumor [67–70]. The combination of the above mentioned PA signal and NIR-II fluorescence imaging can form a complementary imaging mode that provides deeper tissue penetration, higher spatial resolution and stronger supersensitivity for imaging, treatment guidance and postoperative detection of the disease site. However, Ag_2S NPs with different sizes have different photothermal effects and fluorescence characteristics, so the size has a significant influence on the therapeutic and diagnostic effects of Ag_2S NPs.

In this review, we sketched out the synthesis methods and influencing factors of synthesize Ag_2S NPs with different sizes firstly, and then the photothermal effects and fluorescence characteristics of Ag_2S NPs with different sizes were compared. Meanwhile, the relationship between photothermal effects and fluorescence characteristics and particle sizes of Ag_2S NPs were summarized according to the reported articles. Finally, the possibility and challenge of Ag_2S NPs for constructing a theranostic agent were discussed. This review hopes to provide some ideas for the subsequent development of Ag_2S NPs as a single-component theranostic agent or multifunctional nano-carrier to better use and exert its value.

2. Structure and synthesis of Ag_2S NPs

Ag_2S have three convertible crystal structures, including monoclinal Ag_2S (α-Ag_2S), body-centered cubic Ag_2S (β-Ag_2S) and face-centered cubic Ag_2S (γ-Ag_2S) [71,72]. Compared with the cubic Ag_2S, α-Ag_2S is easier to synthesize, and its particle size is smaller, so it can be better used in biomedical applications. Here, we will focus on the Ag_2S of this crystal. With the rapid development of biological nanotechnology, the synthesis technology of Ag_2S materials has also been developing continuously, and numerous nanoparticles with different morphologies, structures, and particle sizes are emerging one after another. This part mainly summarized the structure, synthetic methods and influence factors of Ag_2S NPs with different particle sizes. Table 1 [73–94] mainly lists some Ag_2S NPs with different morphologies and structures, and Fig. 1 shows part of TEM diagram of nanoparticles.

2.1. Synthetic methods of Ag_2S NPs

In 1995, Pileni *et al.* [95] first reported and synthesized Ag_2S NPs with different sizes (<10 nm) by reverse micelle method. Later,

Table 1
Different types of Ag_2S NPs.

Nanoparticle	Morphology	Method of synthesis	Nanoparticle size	Refs.
Ag_2S NCs	Nanocluster	Biomineralization	~2.8 nm	[73]
Ag_2S QDs	Nanocrystal	Seed-growth	4.7 nm	[74]
		Hot-injection	3–10 nm	[75]
Ag_2S NPs	Nanosphere	Solventless thermolytic	12 nm, 20 nm, 50 nm	[76]
Ag_2S NPs	Nano-cubes	Solvothermal	7~50 nm	[77]
Ag_2S NRs	Nanorice	Hydrothermal	70–90 nm	[78]
Ag_2S NPs	Hexagonal	Chemical precipitation	100–120 nm	[79]
Ag_2S NRs	Nanorod	Chemical precipitation	70–160 nm × 200–360 nm	[80]
Ag_2S	Worm-like	W/O reverse microemulsion	30 nm × micrometers	[81]
		Solution-growth	50 nm	[82]
Ag_2S NRs	Rod-like	γ-Ray irradiation	200–500 nm	[83]
Ag_2S MRS	Micro-rod	Solvothermal	~ 0.3 μm	[84]
Ag_2S NWs	Nanowire	Microwave	>10 μm	[85]
		Wet chemical method	10–30 nm × micrometers	[86]
		Solution-growth	150 nm × ~10 μm	[82]
Ag_2S	Spokewise microbar	Solution-growth	2.5-3.0 μm × 60 μm	[82]
Ag_2S NSs	Nanosheet	Hydrothermal	–	[87]
Ag_2S	Tetrahedron	Solvothermal	100–1000 nm	[88]
Ag_2S-ZnS	Core-shell	Photochemical approach	7 nm	[89]
Cu-Ag_2S	Nanosphere	Cation exchange method	8.6 nm	[90]
Ag/Ag_2S	Nanowire	*In-situ* synthesis	9 × 21 nm	[91]
Ag_2S/HgS	Core-shell	Cation exchange method	15–30 nm	[92]
Au@Ag_2S	Core-shell	*In-situ* synthesis	~80 nm	[93]
Ag_2S/Ag	Nanoprism	Cation exchange method	200 nm	[94]

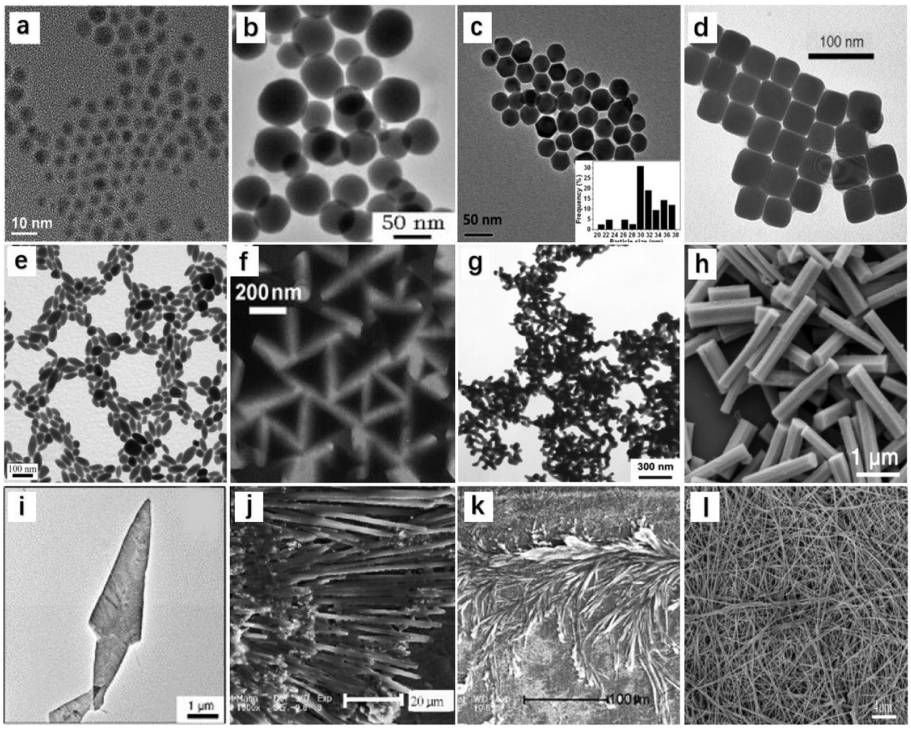

Fig. 1. Different morphologies and structures of Ag_2S nanomaterials. (a) Quantum dots. Copied with permission [74]. Copyright 2012, American Chemical Society. (b) Nanosphere. Copied with permission [75]. Copyright 2012, Elsevier B.V. (c) Hexahedron. Copied with permission [78]. Copyright 2012, Elsevier B.V. (d) Nanocube. Copied with permission [76]. Copyright 2004, WILEY-VCH Veriag GmbH & Co. KGaA, Weinheim. (e) Nanorice. Copied with permission [77]. Copyright 2014, Elsevier B.V. (f) Tetrahedron. Copied with permission [87]. Copyright 2007, WILEY-VCH Veriag GmbH & Co. KGaA, Weinheim. (g) Worm-like. Copied with permission [80]. Copyright 2010, Elsevier B.V. (h) Micro-rod. Copied with permission [83]. Copyright 2019, The Authors. (i) Nanosheet. Copied with permission [86]. Copyright 2005, Elsevier B.V. (j) Spokewise. (k) Nanofibers. (j and k) Copied with permission [81]. Copyright 2007, Elsevier B.V. (l) Nanowire. Copied with permission [85]. Copyright 2008, Elsevier B.V.

Mehra *et al.* [96] synthesized water-soluble Ag_2S NPs with sizes of ~9 nm by modifying cysteine and glutathione in 1999. Subsequently, Zhao [97] and Qian [98] successively prepared Ag_2S NPs with uniform particle size by using dodecythiol as surface ligand molecule and solvent in 2003 and 2004.

The synthetic solvent of Ag_2S NPs includes organic phase and aqueous phase. Organic phase synthesis mainly consists of a high-temperature thermal decomposition method [76,99–102] and solvent thermal method [77,79]. The nanoparticles obtained by the above methods have uniform sizes and good crystal quality. However, the organic solvent is harmful to the human body, and the prepared nanoparticles are hydrophobic, which need further modification to improve the biosafety of those nanoparticles' application *in vivo*. Based on the above problems, more researchers turned to the direct synthesis of Ag_2S NPs in the aqueous phase. At present, common water phase synthetic methods include chemical coprecipitation method [103–106], hydrothermal method [78,107,108], bionic synthesis method [109–114] and cation exchange method [94,115] and so on. Other synthesis methods also include *in situ* growth method [116,117], seed growth method [74], electrostatic spinning method [118], *etc.* Compared with other morphologies of Ag_2S, spherical nanoparticles have been studied more in photothermal therapy and fluorescence imaging, so we briefly summarized partial synthesis methods and applications of this kind of Ag_2S NPs with different sizes in Table 2 [74,99,101,103,107,112,115,118–126].

2.2. Influence factors of different sizes

The physicochemical properties and optical characteristics of the same nanoparticle will change with its particle size, leading to different applications [127,128]. Generally speaking, Ag_2S NPs with different sizes can be obtained by different synthesis methods. However, Ag_2S NPs with different sizes can also be obtained by controlling different conditions of the same method. Therefore, it is our ultimate goal to skillfully control different reaction conditions to form the optimal size in the synthesis of Ag_2S NPs. This section discussed different influence factors of Ag_2S NPs size.

2.2.1. Ag/S ratio

In 2008, when Li *et al.* was synthesizing nanowires, they found that increasing Ag/S would result in enlarging the size of reaction products. However, if the ratio of Ag/S is reduced, Ag_2S nanospheres would appear, and further decreasing would lead to smaller nanospheres [86]. In the same year, Andrew A.R. Watt *et al.* synthesized Ag_2S NPs with different sizes by controlling the ratio of Ag/S (as shown in Fig. 2), which has the same phenomenon as Li's group [129]. Yagci Acar *et al.* developed water-soluble Ag_2S QDs with high luminescence in 2012 [130]. Likewise, they also obtained a series of Ag_2S NPs with different sizes and screened out the optimized luminescent nanoparticles among them. Yu *et al.* [112] studied the relationship between the particle sizes and Ag/S ratios of Ag_2S NPs in detail, which proved the above conclusion once again. As described in Fig. 3, with the Ag/S molar ratios change from 3:1 to 1:10, the nanoparticle size varies from 1.5 nm to 7.5 nm.

It can be seen that the precursors' concentration of Ag^+ and S^{2-} plays a significant part in the nucleation and growth of Ag_2S NPs. In the initial phase of reaction, Ag^+ and S^{2-} continue to combine to form a nucleus with small particle size; In the later stage of the reaction, the nanoparticles begin to grow and the particle size becomes larger and larger. As S^{2-} is constantly added, Ag^+ is consumed and nanoparticles continue to grow. The larger the Ag/S, the smaller the particle size. Conversely, the more S^{2-} is added, the larger the particle size is [79,86,120,130,131].

Table 2
Synthetic methods of Ag_2S nanoparticles and their applications.

Nanoparticles	Precursors	Method	Size	Application	Refs.
Ag_2S QDs	AgAc, $(TMS)_2S$	Hot-injection	1.5 ± 0.4 nm	NIR imaging	[74]
Ag_2S QDs	Ag (DDTC), 1-dodecanethiol	Thermal decomposition	2.8 nm	*In vivo* imaging	[99]
Ag_2S QDs	$AgNO_3$, BSA	Bionic synthesis	2.8 nm	Near-infrared imaging	[112]
Ag_2S QDs	CdS QDs, Ag^+	Cation exchange method	~3.5 nm	NIR-II imaging	[115]
Ag_2S NCs	Ag (DDTC), 1-dodecanethiol	Thermal decomposition	4.3 ± 0.7 nm	*In vivo* imaging	[101]
Ag_2S QDs	Ag (DDTC), 1-dodecanethiol	Thermal decomposition	5.4 nm	NIR-II imaging	[119]
Ag_2S NDs	$AgNO_3$, Na_2S	Biosynthesis	4.1 nm, 7.5 nm, 9.8 nm	Phototherapy, near-infrared imaging	[120]
Ag_2S NPs	Ag (DDTC)	Thermal decomposition	10.2 ± 0.4 nm	NIR-II imaging	[121]
Ag_2S NPs	$AgNO_3$, Na_2S	Biosynthesis	9.0 ± 3.5 nm	–	[122]
Ag_2S NPs	$AgNO_3$, Na_2S	Colloidal method	10–12 nm	Electrical characteristics	[123]
Ag_2S NPs	$AgNO_3$, CS_2	Electrostatic spinning	15 nm	Nanomaterials	[118]
Ag_2S NPs	$AgNO_3$, Na_2S	Ion-exchange method	20 nm	Sono-catalyze	[124]
Ag_2S NPs	$AgNO_3$, Gum Kondagogu	Hydrothermal method	~25 nm	Photocatalytic, fluroscence, and antimicrobial activities	[107]
Ag_2S NPs	$AgNO_3$, Thioacetamide	Wet chemical method	40 nm	Tumor photothermal therapy	[103]
Ag_2S NPs	$AgNO_3$, Na_2S, $NaC_{12}H_{25}SO_4$	Low temperature synthesis	30–60 nm	Electrical conductivity	[125]
Ag_2S NPs	$AgNO_3$, $(CH_2)_2CS$	Hydrothermal method	~100 nm	Photothermal therapy	[126]

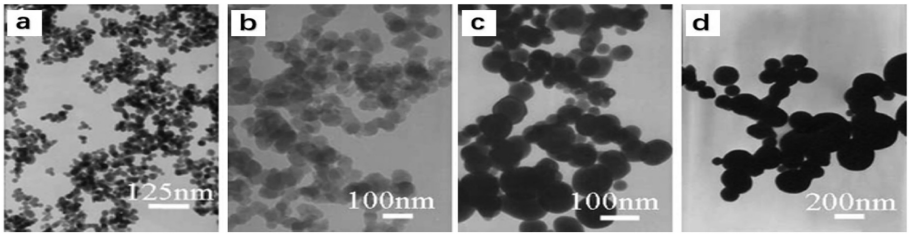

Fig. 2. TEM images of Ag_2S NPs with different Ag/S molar ratios at 180 ℃. (a) 1:1; (b) 2:1; (c) 4:1; and (d) 8:1. Reproduced with permission [128]. Copyright 2008, American Chemical Society.

2.2.2. Reaction time

In a report, the authors prepared Ag_2S carboxyl-terminated nanocrystals by reacting silver nitrate and mercaptopropionic acid [132]. As shown in Fig. 4, two different sizes of nanoparticles were obtained by reacting for 5 min or 30 min at 145 ℃, respectively. Another study, the researchers explored the impact of longer reaction time on the size of nanoparticles [133]. Appropriate amounts of thiourea (Tu) and silver nitrate were mixed and stirred, and then transferred the mixture to Teflon stainless steel autoclave reactor for reaction with 12 h, 24 h, 48 h, 72 h, and 96 h, respectively, at 160 ℃. The results show that the size of nanoparticles increases with the reaction time. A similar pattern was confirmed in Wang's research works in 2014 [134]. With the extension of the reaction time, nanoparticles grow and mature gradually (shown in Fig. 5). Besides, prolonged the reaction time can not only obtain larger size nanoparticles but also improve the crystallinity of nanoparticles continuously, so that the quality of nanoparticles can be optimized [120,130,132,134]. However, the size of particles will be increasing with the continuous extension of reaction time, and their specific surface area and surface energy change, which is easy to cause agglomeration [78,79,133]. Therefore, appropriate reaction time plays a crucial role in the size control of Ag_2S NPs.

2.2.3. Reaction temperature

The reaction temperature has a certain influence on the size of nanoparticles. Meanwhile, the reaction temperature has a significant impact on the crystallinity of nanocrystals. Generally speaking, the higher the temperature, the better the crystallinity and the crystal quality. Some studies suggest that reaction temperature has little effect on nanoparticle size [120,135]. While some reports suggest that the size of nanoparticles increases with the reaction temperature within a certain range [86,129,130]. Wang *et al*. prepared a series of nanoparticles with different size by controlling different reaction temperature (Fig. 5) [134]. After observation and comparison, we found that within a certain range, the higher the reaction temperature, the larger the particle size of the product. However, too high temperature will result in changes in the crystal form of nanocrystals, which lead to increase surface defects or excess, and decrease fluorescence intensity and quantum yield of nanocrystals. Choosing the right reaction temperature is also crucial.

2.2.4. The dosage of ligand

The long-term stability of nude Ag_2S NPs is not ideal. Therefore, the ligand molecules are generally added as stabilizer to modify Ag_2S NPs in the process of reaction, to enhance its stability and water solubility, which facilitate its late clinical application *in vivo*. Besides, the ligand molecules in the reaction also play the role of end-capping reagent, controlling the size of the product nanoparticles.

Xu *et al*. exploited a novel one-pot procedure to generate size-adjustable Ag_2S NPs by pyrolyzed single precursor $Ag[S_2P(OR)_2]$, where $R = C_nH_{2n+1}$ and n value varies from 5 to 20 [136]. In the experiment, Ag_2S NPs of different sizes were synthesized by controlling different n values (n = 8, 12, and 16). As depicted in results, the particle sizes are tunable due to alter the value of "n". According to references [137,138], the same conclusion that particle size increases with the increase of ligand molecule dosage or concentration can be drawn. The increase of the amount of ligand molecule provides more opportunities to react with the surface groups of Ag_2S NPs, thus leading to more adsorption on the surface of nanoparticles, which not only increases the particle size of nanoparticles, but also reduces the surface defects of nanoparticles, and improves their fluorescence intensity and quantum yield. However, from the introduction of part 3, we realized that

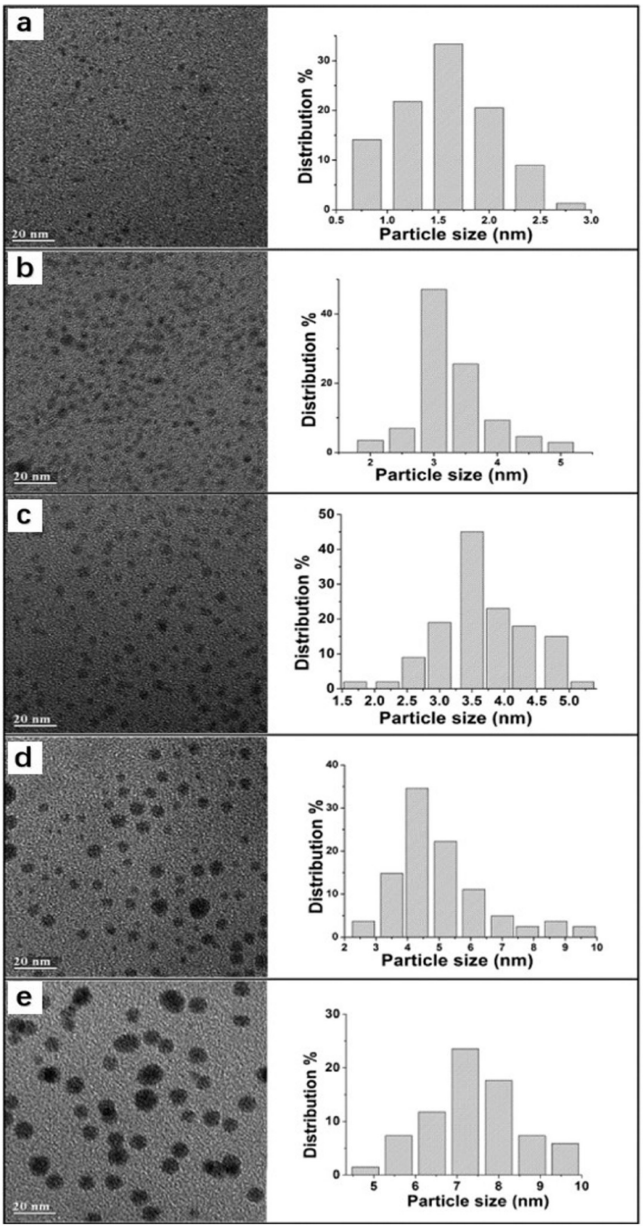

Fig. 3. TEM images and corresponding size distribution histogram of Ag_2S NPs obtained with different Ag/S molar ratios. (a) 3:1; (b) 1:2; (c) 1:3; (d) 1:5; and (e) 1:10. Copied with permission [111]. Copyright 2013, IOP Publishing Ltd. Printed in the UK & the USA.

the size of nanoparticles is inversely proportional to the fluorescence intensity, so controlling the number of ligand molecules can achieve higher diagnostic value.

2.2.5. Other factors

Except for the above factors, the solvent type, pH value, the type and molecular of ligand, and the injection order of ions of the reaction system also have a certain impact on the size of the target particle [135,139–142]. Controlling different reaction conditions can produce very different results for chemical reactions. For example, Havva Yagci Acar *et al.* obtained a series of Ag_2S NPs with different sizes by controlling different reaction pH values [143]. The size of the nanoparticles obtained in the weakly alkaline environment (pH 9.0) was the smallest, and the largest in the acidic environment (pH 5.5).

Through the exploration of the above reaction conditions, it is not difficult to summarize the influence of each reaction condition on the size of nanoparticles. Meanwhile, some reported studies have confirmed our conclusion. Jin *et al.* [115] obtained a series of biocompatible Ag_2S QDs of near-infrared emission by cation exchange method, and detected photoluminescence emission spectra of Ag_2S QDs at different reaction time points. As we said above, with the passage of reaction time, the size of nanoparticles became larger, and the corresponding position of maximum emission peak experienced redshift. Similarly, Pang *et al.* [74] also obtained a series of Ag_2S QDs with different emission peaks, which again confirmed the relationship between reaction temperature, time and particle size. According to reference [110], the effect of the Ag/S ratio on particle sizes is also consistent with the above conclusions.

3. Nanoparticles with different sizes for photothermal therapy

Photothermal therapy, as a novel tumor treatment method, is expected to become another tumor treatment method with great potential after surgical resection, radiotherapy and chemotherapy due to its noninvasive treatment, low level of systemic side effects, and the conquest of chemotherapy drug resistance at tumor sites [144–151]. Recently, there are more and more researches about photothermal materials, among which gold nanomaterials are the main ones (Figs. 6a and b). However, due to the high cost, poor photothermal stability and biometabolicity *in vivo* of gold nanomaterials, many other photothermal materials have emerged in recent years. Among them, metal-sulfur compounds, such as CuS and Ag_2S, have become the new research hotspot of photothermal materials because of their low cost, good photothermal stability, low cytotoxicity and controllability of particle size morphology [18]. While, compared with CuS materials with the higher basal

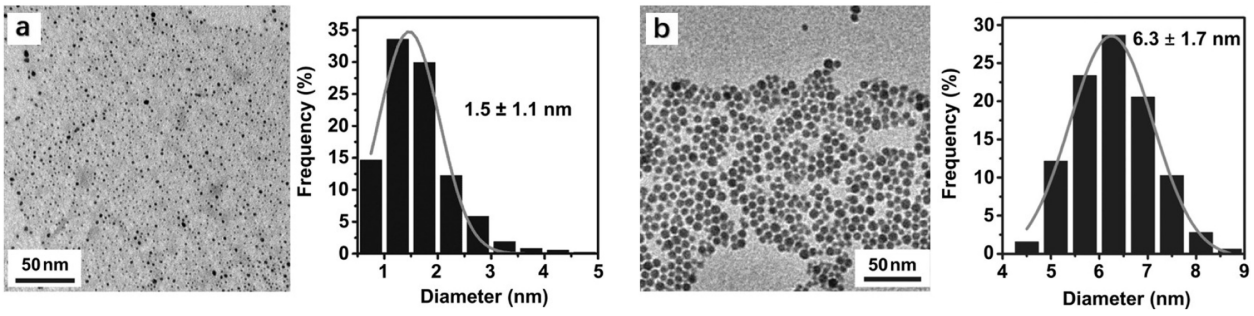

Fig. 4. TEM images and size distribution graphs of Ag_2S nanocrystals synthesized at 145 °C for different reaction times. (a) 5 min; (b) 30 min. Reproduced with permission [133]. Copyright 2012, Elsevier B.V.

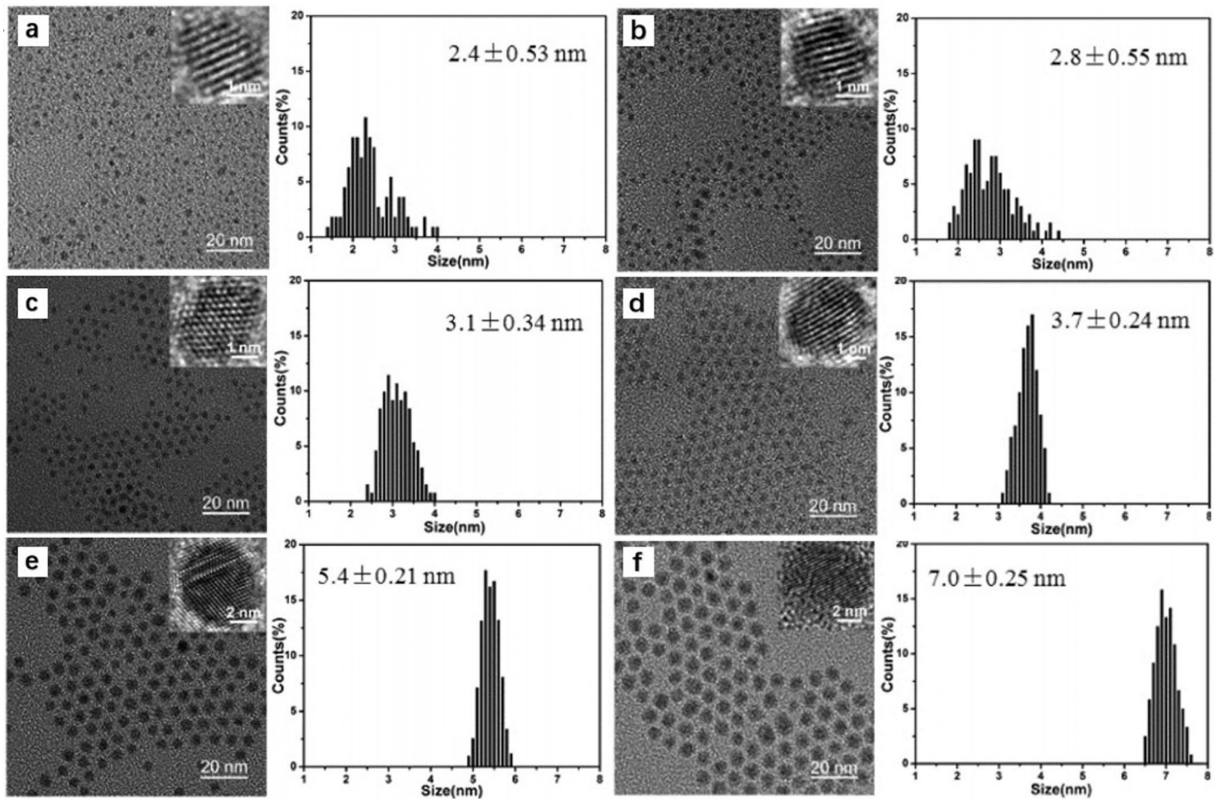

Fig. 5. TEM and HRTEM images (inset) and correspondingly size distribution histograms of Ag_2S nanocrystals synthesized for different reaction times. (a) 130 °C, 1 min; (b) 140 °C, 2 min; (c) 160 °C, 3 min; (d) 180 °C, 2 min; (e) 210 °C, 60 min; and (f) 230 °C, 60 min. Reproduced with permission [132]. Copyright 2014, American Chemical Society.

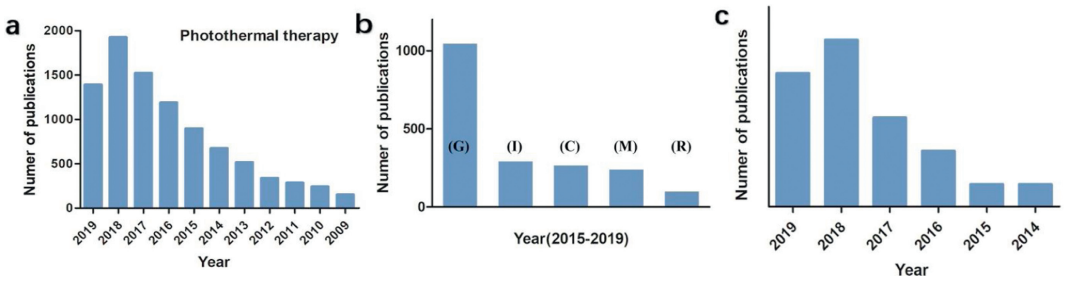

Fig. 6. (a) The reseach trend and publications of photothermal therapy in recent ten years. (b) The publications of several common photothermal materials during 2015 to 2019. G: Gold nanomaterials (1054); I: ICG (301); C: Carbon-based materials (274); M: Metal-sufur compounds (248); R: IR dyes (108). (c) The research trend of Ag_2S nanomaterials in last 5 years. All data are obtained from web of science keyword search.

heat, Ag_2S has better biocompatibility, biometabolicity, lower toxic and side effects, and higher photothermal conversion efficiency. Therefore, more and more researchers are turning their attention to the photothermal effects of Ag_2S in recent years (Fig. 6c).

3.1. Ag_2S quantum dots

A nanoparticle is called a quantum dot when its size is no larger than twice the Bohr radius. Therefore, the Ag_2S quantum dots discussed in this section are less than 4.5 nm in size [134]. Initially, Ag_2S quantum dots were mainly used for near-infrared imaging, but with the continuous research, some Ag_2S quantum dots began to be used for photothermal treatment. In 2016, Cai *et al.* [109] developed a straightforward method to directly synthesize water-soluble Apt43-Ag_2S QDs with 2.5 nm. As shown in Fig. 7a, the temperature of Apt43-Ag_2S QDs solution (100 μg/mL) can be elevated by almost 30 °C irradiated by 808 nm laser (1.0 W/cm^2, 12 min). The QDs exhibited concentration-dependent and power-dependent photothermal effect, good photothermal conversion efficiency (23.8%) and excellent photothermal stability (Figs. 7b and c). After intravenously injected with 250 μL of Ag_2S QDs (400 μg/mL) for 3 h, the tumor-bearing nuked mouse were irradiated by 808 nm laser (1.5 W/cm^2, 10 min). As shown in Figs. 7d and e, the temperature of the tumor sites reached approximately 52 °C. And the tumors can be effectually ablated with no longer growth (Figs. 7f–h). Later, Chen and co-workers [120] synthesized Ag_2S nanodots (4.1 nm) by biomineralization (Fig. 8a), which had good photothermal conversion efficiencies (33.7%–35.0%). In 2018, Liu *et al.* [65] developed a multifunctional Ag_2S QD@PC_{10}ARGD hybrid nanogel with high QY (4.3%). In this study, the temperature of nanogel solution contained 4.5 nm Ag_2S QDs (1.0 mg/mL, Ag^+ ions) increased significantly compared with

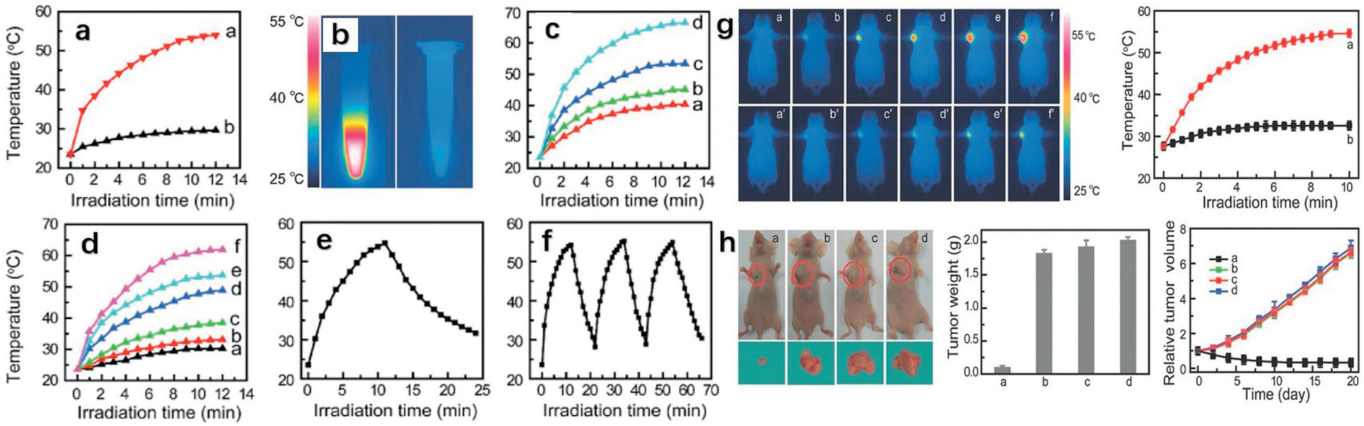

Fig. 7. Temperature-elevation curves (a) and infrared themography (b) of Apt43-Ag_2S QDs and Apt43 solution. (c, d) Dependence of the temperature-elevation curve profiles on the concentration of Apt43-Ag_2S QDs solution and power densities of laser. (e, f) The course of temperature and photothermal stability of QDs solution. (g) Infrared themography and temperature elevation of tumor sites *in vivo*. (h) Tumor size, tumor weight, and relative tumor volume of the mice in experiment. Reproduced with permission [108]. Copyright 2016, WILEY-VCH Verlag GmbH & Co. KGaA, Weinheim.

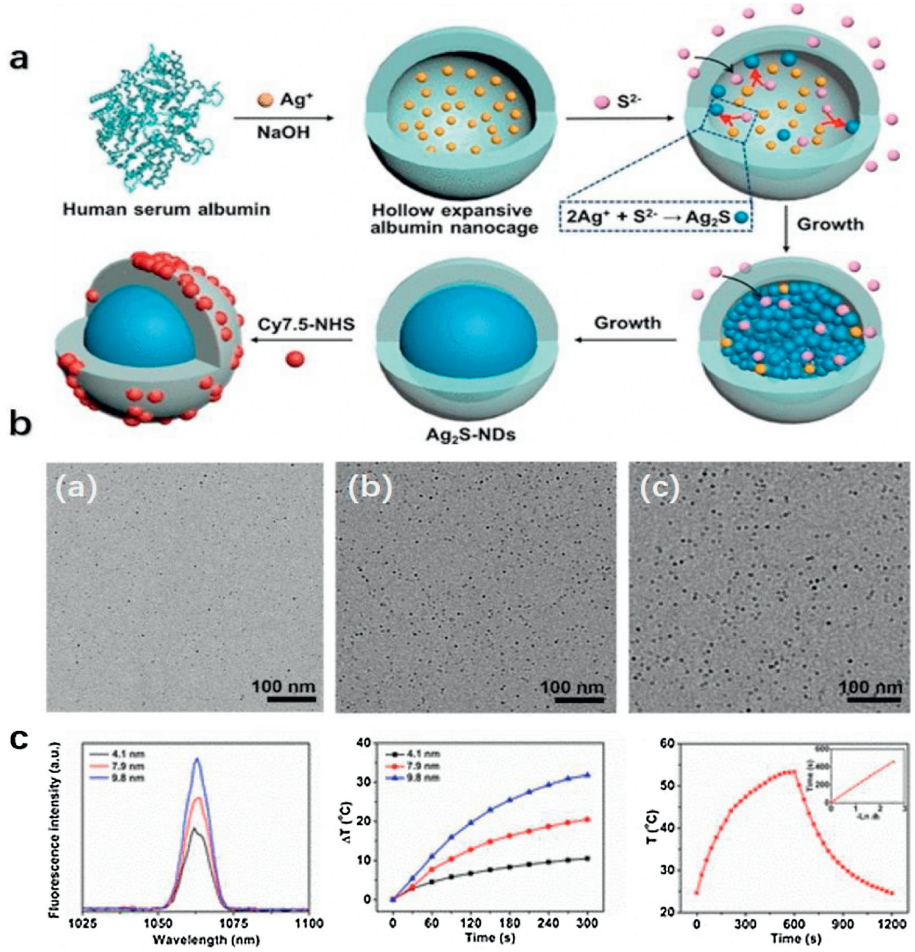

Fig. 8. (a) Schematic illustration of Ag_2S@GSH nanodots by biomimetic synthesis. (b) TEM images of Ag_2S-NDs. (a. 4.1 nm, b. 7.9 nm, c. 9.8 nm). (c) Absorption spectra and photothermal properties of Ag_2S-NDs. Reproduced with permission [119]. Copyright 2017, American Chemical Society.

the PC_{10}ARGD aqueous solution with an 810 nm laser (2.5 W/cm^2, 8 min) (Figs. 9a and b), and nanogel showed good photothermal conversion efficiency (Fig. 9c). The temperature of tumor sites reach up to 60.7 ℃ rapidly under the irradiation of 810 nm laser (2.5 W/cm^2, 2 min), which can effectively scald tumor tissue (Figs. 9d and e). Zhu *et al.* [116] fabricated a versatile nano platform, in which Ag_2S as the diagnostic agent and photothermal agent, was synthesized on mesoporous silica by *in situ* growth method. The multifunctional Ag_2S@HMSs-A7R displayed a great photothermal effect. The temperature increased to roughly 54.3 ℃ in tumor sites under irradiated by 808 nm laser (1.0 W/cm^2, 10 min), which was enough to kill the tumor cells.

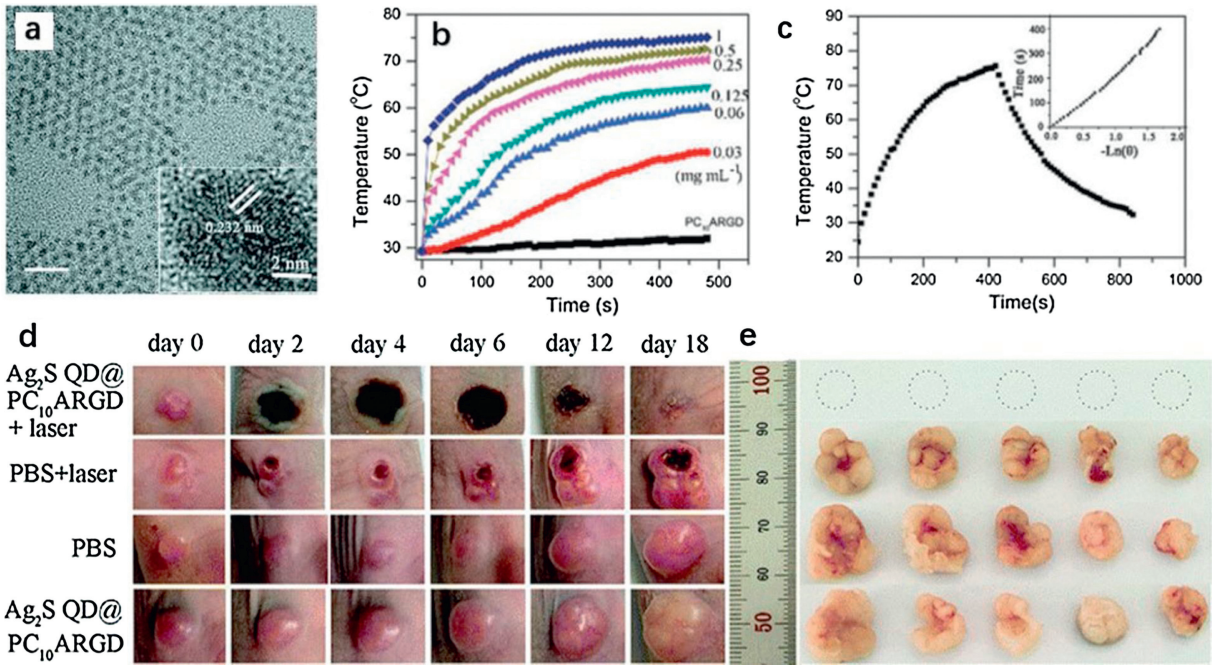

Fig. 9. (a) TEM and HRTEM images of hydrophobic Ag_2S QDs with 4.5 nm. (b) Temperature elevation curves of Ag_2S QD@PC10ARGD with various concentrations. (c) Photothermal conversion efficiency of Ag_2S QD@PC10ARGD. (d, e) The anti-tumor effect of all experimental groups. Reproduced with permission [64]. Copyright 2018, The Royal Society of Chemistry.

3.2. Ag_2S nanosphere

In addition to Ag_2S quantum dots, Ag_2S nanospheres of a certain size show better photothermal effects. In 2018, Zhao's group [152] constructed a multifunctional co-delivery drug and gene nano-platform, in which Ag_2S acts as a fluorescent tracer and photo-thermal agent. In this work, the particle size of Ag_2S NPs is 6.5 nm, with a good photothermal effect. The nude mice bearing tumor (group V) were injected with 50 μL of nanoprobe (20 mg/mL) intratumorally and irradiated by 808 nm laser (2.0 W/cm^2, 10 min) at 24 h post-injection. The temperature of the tumor site reached 54.4 ℃, and the effect of anti-tumor is the most effective. What is more, Chen and co-workers [120] also synthesized Ag_2S nanodots of 7.5 nm and 9.8 nm by biomineralization (Fig. 8b), which had similar photothermal conversion efficiencies (33.7%–35.0%). Meanwhile, those nanodots have been revealed a size-dependent photothermal effect. Among them, 9.8 nm Ag_2S shows better photothermal effect, as described in Fig. 8c. Then, they studied the antitumor effect of 9.8 nm Ag_2S-NDs *in vivo*. Different doses of Ag^+ (10.0, 30.0 and 50.0 μmol/kg) were injected to the tumor-bearing mice, followed by irradiated by 785 nm laser (1.5 W/cm^2, 5 min) at 24 h after the first injection. The temperature elevation of the maximum dose at tumor sites is about ~19.0 ℃, which resulted in completely tumor ablation without recurrence. In 2015, Chen *et al*. obtained Ag_2S nanomaterials with particle size of ~100 nm. The nanoparticle had an excellent photothermal conversion efficiency (reach up to 63%) and showed a great photothermal property [126].

3.3. Other morphologies of Ag_2S

So far, the photothermal effect of spherical Ag_2S NPs has been confirmed by some researchers, but the application of other morphologies of Ag_2S NPs in photothermal therapy has not been reported. Nevertheless, inspired by other photothermal nano-materials (like Au) with different morphologies, it also reminds us that there is still a lot of work to be done to make the best use of Ag_2S materials.

4. The fluorescence characteristics of Ag_2S NPs with different sizes

The early researches of Ag_2S materials are mainly focused on photo-electrochemistry, biosensor, and catalytic application [123,153–158]. Although Ag_2S with different sizes have been synthesized and the concept of Ag_2S quantum dots has even been proposed [159], the fluorescence characteristics of Ag_2S materials were first reported until 2010 [121]. Wang *et al.* synthesized Ag_2S QDs with uniform sizes by thermal decompose the single precursor of Ag (DDTC) and studied its near-infrared fluorescence emission characteristics. Hence, the door for the use of Ag_2S nanomaterials in near-infrared imaging was opened. Recently, there are more and more reports on near-infrared fluorescence imaging of Ag_2S nanomaterials. Efforts have been made to prepare Ag_2S QDs with stronger fluorescence signals, higher quantum yield and better crystal quality [89,125,160,161]. In this section, we summarized the fluorescence characteristics of Ag_2S NPs with different sizes.

4.1. The position of emission peak

Wang's group proposed the NIR-II fluorescence of Ag_2S firstly, and they also have done a lot of work on Ag_2S nanomaterials. In 2014, Wang *et al*. synthesized a battery of high-quality Ag_2S QDs successfully by means of pyrolysis of single-source precursor of Ag (DDTC), as shown in Fig. 10a [134]. The particle from 2.4 nm to 7.0 nm exhibited a size-dependent for optical characteristics. The maximum emission peak of Ag_2S QDs shifted from 975 nm to 1175 nm (Fig. 10b). H. Yagci Acar *et al.* presented a simple, one-step method synthesis of biocompatible Ag_2S-PEG QDs in 2016 [162]. In this study, Ag_2S QDs with different particle sizes from 2.2 nm to 2.6 nm were obtained by controlling diverse reactant ratios. As described in the results, the maximum emission peak can be tuned from 775 nm to 915 nm with the increase of nanoparticles.

Cai *et al*. successfully synthesized Apt43-Ag_2S QDs of the sizes ~2.5, 3.1 and 4.4 nm, whose photoluminescence emission correspondingly displays symmetric emission peaks at ~978, 1072 and

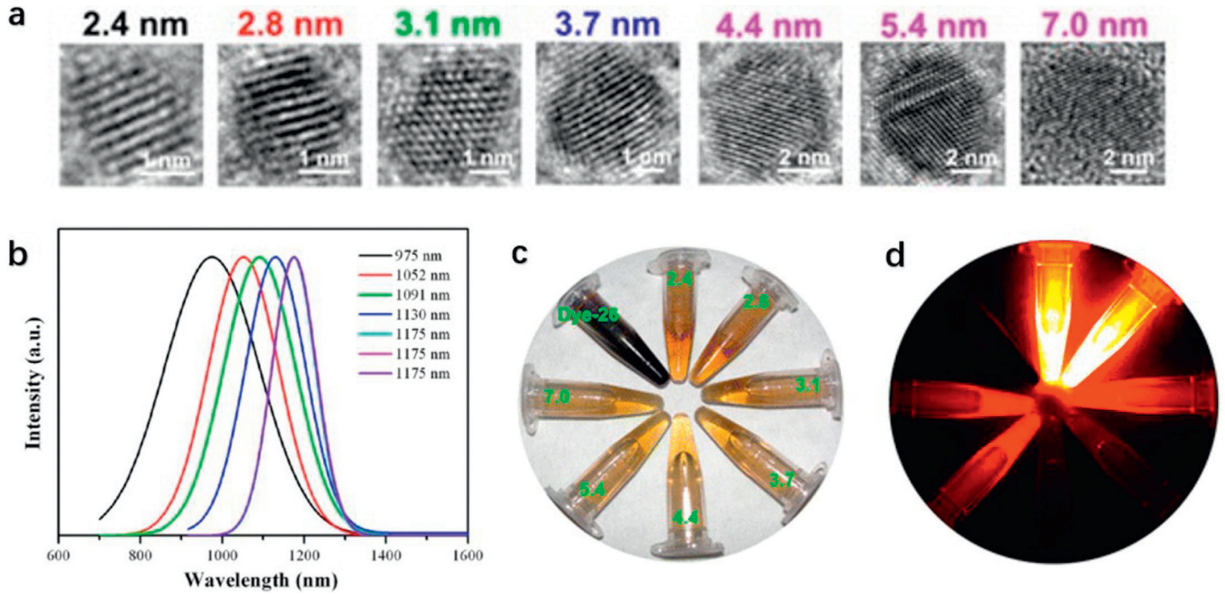

Fig. 10. (a) HRTEM images of Ag_2S QDs with different sizes. (b) PL emission spectra of as-prepared Ag_2S QDs under irradiated by 785 nm laser. (c) Brightfield images and (d) NIR-II fluorescence images of Ag_2S QDs with different sizes. Reproduced with permission [132]. Copyright 2014, American Chemical Society.

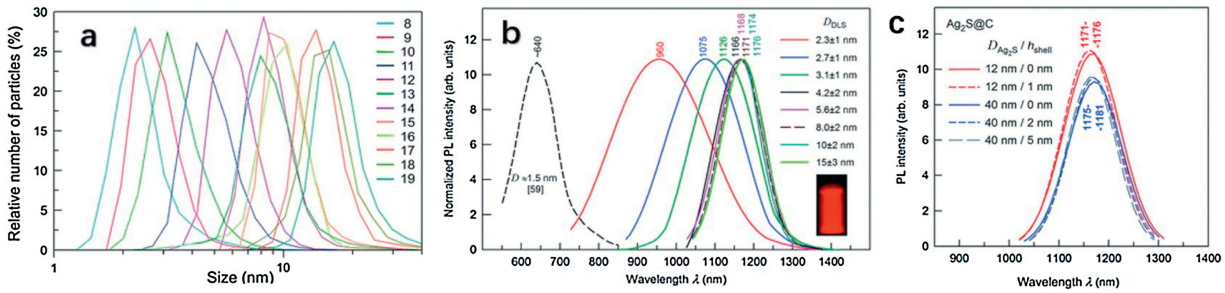

Fig. 11. (a) The different particle sizes of Ag_2S quantum dots measured by DLS. (b) The PL emission spectra of Ag_2S QDs size DDLS from 2.3 nm to 17.0 nm. (c) The PL emission spectra of Ag_2S@C NPs with different citrate shell thickness. Reproduced with permission [163]. Copyright 2017, The Royal Society of Chemistry.

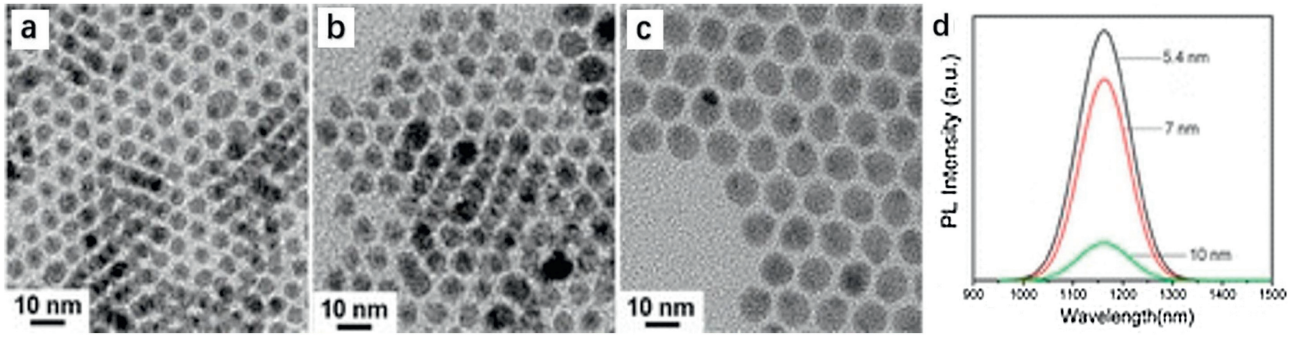

Fig. 12. (a-c) TEM images of Ag_2S QDs with the size from 5.4 nm to 10 nm. (d) The PL intensity of above-mentioned Ag_2S QDs. Copied with permission [164]. Copyright 2012, American Chemical Society.

1179 nm [120]. In 2017, I. Gusev *et al.* reviewed a series of Ag_2S NPs with different sizes and summarized their fluorescence emission spectrum. As shown in Figs. 11a and b, the photoluminescence emission peaks tunable from ~640 nm to 1176 nm with the sizes of Ag_2S QDs increase from 1.5 nm to 15 ± 3 nm [163,164]. Another work, water-soluble Ag_2S QDs with different sizes were one-pot synthesized, and their emission peaks tunable from 1050 nm to 1294 nm with the sizes change from 1.6 nm to 6.8 nm [112]. In 2011, Pang *et al.* presented two different sizes Ag_2S QDs of 1.5 nm and 4.6 nm which have a tunable emission from 690 nm to 1227 nm [74]. Subsequently, they reported a series of Ag_2S QDs with a tunable emission from 510 nm to 1221 nm by increasing the sizes of Ag_2S QDs from 1.5 ± 1.1 nm to 6.3 ± 1.7 nm [132]. In summary, within a certain range (< 4.5 nm), the smaller the particle size, the shorter the wavelength of maximum emission peak. While the size of nanoparticles continues to increase (< 40 nm), the position of the

Table 3
Functional modification of Ag_2S NPs.

Nanoparticle	Ligand	The function of ligand	Refs.
Ag_2S@BSA-antiVEGF	BSA	Reactor, water-solubility modification	[110]
Ag_2S@BSA-DTPA^{Gd} pQDs	BSA-DTPA^{Gd}	Reactor, MRI contrast agent	[111]
Ag_2S@BSA	BSA	Reactant, reactor	[174]
Ag_2S@GSH	GSH	Water-solubility modification	[175]
Ag_2S-CS-SNO	GSH	Reactant, reactor	[113]
Apt43-Ag_2S QDs	Apt43	Reactor and active targeting ligand	[109]
Ag_2S-PEG	PEG	Water-solubility modification	[99]
RNase A-Ag_2S QDs	RNase A	Capping agent	[169]
Ag_2S@PVP	PVP	Blocking agent	[176]
Ag_2S@PVP	PVP	Reactor, blocking agent	[104]
Ag_2S QDs	PMAO	Water-solubility modification	[177]
Ag_2S cRGD	3-MPA, cRGD	Water-solubility modification	[178]
Ag_2S-AMD3100 QDs	3-MPA, AMD3100	Active targeting ligand	[108]
Ag_2S-I@DSPE-PEG2000-FA	PEG2000, FA		[100]
FA-PEG-Ag_2S QDs	PEG, FA		[179]
Ag_2S@Ald QDs	PEG, Ald		[180]
T&D@RGD-Ag_2S	PEG, cRGD		[181]
Ag_2S@PC_{10}ARGD	PC10A, RGD		[65]

maximum emission peak is no longer red shifted. The same phenomenon has been widely reported in other researchers' work [100,102,110,165].

4.2. The intensity of photoluminescence

From the discussion in the previous part, we have known the relationship between the particle size and the position of emission peak. In this section, we will discuss the effect of nanoparticle size on fluorescence signal intensity.

Wang *et al*. synthesized Ag_2S QDs with different sizes that have different fluorescence intensity, as described in Figs. 10c and d. The images appear to show that the smaller the particle size (particle size less than 4.4 nm), the stronger the intensity of photoluminescence. However, when the particle size is larger than 4.4 nm and smaller than 7.0 nm, the signal intensity of nanoparticles increases slightly. The same conclusion can be drawn from their previous work (Fig. 12) [166]. I. Gusev *et al*. also studied Ag_2S materials with different particle sizes, and the photoluminescence intensity showed the same trend (Fig. 11c). The fluorescence signal intensity of Ag_2S NPs with different sizes synthesized by H. Yagci Acar *et al*. also decreased with the increase of particle size, but the fluorescence intensity of nanoparticles with the smallest particle size was the smallest, which may be attributed to the serious surface defects. Most recently, Wang *et al*. proposed a new solvent tailored strategy to synthesize ultrasmall Ag_2S QDs with strong NIR-II luminescence. In their works, they prepared a number of Ag_2S QDs with different particle sizes in different reaction solvent [Oam: (a1) 8.3 + 1.8 nm, (a2) 7.8 + 1.0 nm, (a3) 6.5 + 0.7 nm; DDT: (b1) 9.0 + 1.5 nm, (b2) 5.5 + 0.7 nm, (b3) 5.0 + 0.6 nm; Glycerin: (c1) 8.1 + 1.1 nm, (c2) 5.4 + 0.9 nm, (c3) 3.7 + 0.6 nm], and compared their fluorescence spectrum [167]. It is not difficult to see from the experimental results that the intensity of the maximum emission peak has a negative correlation to the particle size.

5. Safety evaluation of Ag_2S materials

As for the biosafety evaluation of Ag_2S materials, it does not contain harmful ions like other sulfur compounds, such as PdS, CdS, CdSe. Besides, it is reported that Ag_2S QDs did not show any cytotoxicity or DNA damage to V97 cells within the allowable range of the medically relevant dose [168]. Ag_2S QDs did not change the apoptosis of cells and had a good biocompatibility. Meanwhile, the solubility product constant of Ag_2S is ultralow ($K_{sp} = 6.3 \times 10^{-50}$), and the amount of Ag ions released into the biological environment in the body is minimum, which also ensures its biosecurity [169,170]. Also, Ag^+ also has an antibacterial effect, which can inhibit bacterial infection and proliferation to a certain extent *in vitro* experiments, belonging to environmentally friendly materials [171,172].

In addition to the safety guarantee of nanoparticles themselves, surface modification can further enhance their biocompatibility and biosecurity [173]. For example, some Ag_2S NPs synthesized in the organic phase have poor water solubility, which can be modified by some hydrophilic ligands, such as PEG, PVP, protein, to facilitate *in vivo* and *in vitro* experiments. What is more, modification of some active targeting ligands can improve the focus targeting of nanoparticles, thereby shortening their circulation time *in vivo*, reducing the release of metal ions *in vivo*, and avoiding their accumulation of toxic and side effects in other organs, so that they can play a faster, more and more effective therapeutic effect. Several types of functionalized Ag_2S NPs are shown in Table 3 [65,99,100,104,108–111,113,174–181].

6. Conclusions and challenges

Theranostics integrates the functions of diagnosis and treatment, so it has obvious advantages over a single diagnosis or treatment. Ag_2S can emit fluorescence in the form of light energy and also can raise the temperature in the form of heat energy to release absorbed energy after absorbing near-infrared light. The combination of photoacoustic signal and fluorescence characteristics of Ag_2S can provide better imaging depth, spatial resolution and more accurate anatomical information. At the same time, it can also kill tumor cells by its own photothermal effect. Here, we listed some synthesis methods and influence factors of sizes of Ag_2S nanomaterials briefly. Next, we summarized and compared the photothermal effects and fluorescence characteristics of Ag_2S with different particle sizes. It can be seen that the photothermal effect and fluorescence characteristics of Ag_2S NPs are correlated with the particle size. Namely, within a certain size range (< 100 nm), the photothermal effect of Ag_2S NPs is directly proportional to the particle size, and there is a dependence of concentration, laser power and irradiation time. Meanwhile, within a certain range of particle size (< 4.5 nm), the fluorescence emission peak redshifts with the increase of particle size, and the intensity of fluorescence emission peak first increases and then decreasesin the range of particle size (< 40 nm). Currently, there are many studies on using Ag_2S QDs for NIR-II imaging, but relatively few reports on

photothermal therapy of Ag_2S. Hence, the value and application of Ag_2S will be fully utilized if the above two are well combined. So it is very important to synthesize Ag_2S NPs with appropriate size, which can better play the role of single-component theranostic agents.

Although Ag_2S is a powerful single-component theranostic agent, there are still some challenges. Firstly, Ag_2S kill tumor tissue mainly through photothermal effect, which has non-invasive and good compliance. However, due to the three-dimensional distribution of tumor internal temperature, it is difficult to completely eliminate tumor tissue by photothermal therapy alone, which will lead to tumor recurrence or metastasis. Therefore, it is suggested that photothermal therapy could be combined with other therapies, such as chemotherapy or immunotherapy, to achieve a thorough therapeutic effect. Secondly, small animal near-infrared imaging equipment in NIR-II is not yet common, which also brings some limitations to relevant studies, and the clinical application in the later stage will also face a long way to go. Fortunately, 3D live animal imaging technology combining NIR-II imaging and photoacoustic imaging has appeared in the market, and its application prospect is quite broad. Meanwhile, there are more and more researches on the second and third region of near-infrared, and it is believed that the equipment problem will be solved soon in the future. This means that fluorescence combined with photoacoustic imaging for clinical diagnosis is expected. In conclusion, Ag_2S NPs has great potential to become a new single-component theranostic agent and an excellent drug carriers of combination therapy.

Declaration of competing interest

The authors declared that they have no conflicts of interest to this work.

Acknowledgments

This work was financially supported by the National Natural Science Fund for Distinguished Young Scholar (No. 31525009), The National Key Research and Development Program of China (No. 2017YFC1103502), National Natural Science Foundation of China (Nos. 31771096 and 31871008), and 1·3·5 Project for Disciplines of Excellence, West China Hospital, Sichuan University (No. ZYGD18002).

References

[1] J.U. Menon, P. Jadeja, P. Tambe, et al., Theranostics 3 (2013) 152–166.
[2] P. Huang, L. Bao, C. Zhang, et al., Biomaterials 32 (2011) 9796–9809.
[3] M.F. Kircher, A. de la Zerda, J.V. Jokerst, et al., Nat. Med. 18 (2012) 829–834.
[4] Z. Wang, P. Huang, O. Jacobson, et al., ACS Nano 10 (2016) 3453–3460.
[5] C. Yang, J. Xu, D. Yang, et al., Chin. Chem. Lett. 29 (2018) 1421–1424.
[6] Y. Wang, T. Yang, H. Ke, et al., Adv. Mater. 27 (2015) 3874–3882.
[7] X. Yang, B.P. Venkatesulu, L.S. Mahadevan, et al., J. Biomed. Nanotechnol. 14 (2018) 809–828.
[8] Z.L. Cheng, A. Al Zaki, J.Z. Hui, V.R. Muzykantov, A. Tsourkas, Science 338 (2012) 903–910.
[9] R.A. Revia, Z.R. Stephen, M. Zhang, Acc. Chem. Res. 52 (2019) 1496–1506.
[10] Y.H. Xu, Y.L. Shan, Y.X. Zhang, et al., Nanotechnology 30 (2019) 425102.
[11] H. Kim, G. Kwak, K. Kim, H.Y. Yoon, I.C. Kwon, Biomaterials 213 (2019) 119207.
[12] B. del Rosal, D. Ruiz, I. Chaves-Coira, et al., Adv. Funct. Mater. 28 (2018) 1806088.
[13] X. Huang, M.A. El-Sayed, J. Adv. Res. 1 (2010) 13–28.
[14] X. Ding, C.H. Liow, M. Zhang, et al., J. Am. Chem. Soc. 136 (2014) 15684–15693.
[15] X.H. Huang, I.H. El-Sayed, W. Qian, M.A. El-Sayed, J. Am. Chem. Soc. 128 (2006) 2115–2120.
[16] S. Sun, L. Zhang, K. Jiang, A. Wu, H. Lin, Chem. Mater. 28 (2016) 8659–8668.
[17] S.T. Lu, D. Xu, R.F. Liao, et al., Comput. Struct. Biotechnol. J. 17 (2019) 619–627.
[18] H. Yang, H. Liang, Y. Xie, Q. Chen, Chin. Chem. Lett. 29 (2018) 1528–1532.
[19] J.Y. Chen, D.L. Wang, J.F. Xi, et al., Nano Lett. 7 (2007) 1318–1322.
[20] T. Niidome, M. Yamagata, Y. Okamoto, et al., J. Control. Release 114 (2006) 343–347.
[21] K.O. Boakye-Yiadom, S. Kesse, Y. Opoku-Damoah, et al., Int. J. Pharm. 564 (2019) 308–317.
[22] J.T. Robinson, K. Welsher, S.M. Tabakman, et al., Nano Res. 3 (2010) 779–793.
[23] D.J. Li, W. Nie, L. Chen, et al., J. Biomed. Nanotechnol. 14 (2018) 2003–2017.
[24] J. Liu, X.P. Zheng, Z.J. Gu, C.Y. Chen, Y.L. Zhao, Nanomed. Nanotechnol. Biol. Med. 12 (2016) 486–487.
[25] M. Zhou, R. Zhang, M.A. Huang, et al., J. Am. Chem. Soc. 132 (2010) 15351–15358.
[26] L. Wang, X.F. Xu, X.G. Mu, et al., Nanotechnology 30 (2019) 415101.
[27] Z. Sheng, D. Hu, M. Zheng, et al., ACS Nano 8 (2014) 12310–12322.
[28] T. Li, C. Li, Z. Ruan, et al., ACS Nano 13 (2019) 3691–3702.
[29] C.Y. Hu, F. Fan, Y. Qin, et al., J. Biomed. Nanotechnol. 14 (2018) 2018–2030.
[30] Y.F. Xiao, F.F. An, J.X. Chen, et al., Small 15 (2019) e1903121.
[31] A. Jordan, R. Scholz, K. Maier-Hauff, et al., J. Neurooncol. 78 (2006) 7–14.
[32] B. Liu, H. Zhang, Y. Ding, Chin. Chem. Lett. 29 (2018) 1725–1730.
[33] N.S. Gao, J.P. Nie, H.F. Wang, et al., J. Biomed. Nanotechnol. 14 (2018) 1883–1897.
[34] Y. Wang, Y. Song, G. Zhu, D. Zhang, X. Liu, Chin. Chem. Lett. 29 (2018) 1685–1688.
[35] R. Toy, L. Bauer, C. Hoimes, K.B. Ghaghada, E. Karathanasis, Adv. Drug Deliv. Rev. 76 (2014) 79–97.
[36] Y. Dai, H. Xiao, J. Liu, et al., J. Am. Chem. Soc. 135 (2013) 18920–18929.
[37] J.M. Niers, J.W. Chen, G. Lewandrowski, et al., J. Am. Chem. Soc. 134 (2012) 5149–5156.
[38] A.K. Rengan, M. Jagtap, A. De, R. Banerjee, R. Srivastava, Nanoscale 6 (2014) 916–923.
[39] S. Khademi, S. Sarkar, A. Shakeri-Zadeh, et al., Int. J. Biochem. Cell Biol. 6 (2011) 2859–2864.
[40] A.J. Einstein, M.J. Henzlova, S. Rajagopalan, J. Am. Med. Assoc. 298 (2007) 317–323.
[41] Z. Sheng, B. Guo, D. Hu, et al., Adv. Mater. 30 (2018) 1800766.
[42] J. Zhao, D. Zhong, S. Zhou, J. Mater. Chem. B 6 (2018) 349–365.
[43] M. Mahmoudi, V. Serpooshan, S. Laurent, Nanoscale 3 (2011) 3007–3026.
[44] F. Ding, Y. Fan, Y. Sun, F. Zhang, Adv. Healthc. Mater. 8 (2019) 1900260.
[45] D.H. Huang, S.Y. Lin, Q.W. Wang, et al., Adv. Funct. Mater. 29 (2019) 1806546.
[46] Kenry, Y. Duan, B. Liu, Adv. Mater. 30 (2018) 1802394.
[47] P.T. Buz, F.D. Duman, M. Erkisa, et al., Nanomedicine 14 (2019) 969–988.
[48] Y.F. Hu, J.J. Zhao, X.F. Li, S.L. Zhao, New J. Chem. 43 (2019) 11510–11516.
[49] R.A. Kumar, M. Prasad, G.K. Kumar, M. Venkateswarlu, C. Rajesh, Phys. Scr. 94 (2019)115806.
[50] N. Samadi, S. Narimani, Anal. Bioanal. Chem. Res. 6 (2019) 47–57.
[51] J.C. Wang, G.B. Gao, F.F. Yang, et al., J. Nanopart. Res. 21 (2019) 50.
[52] X.X. Hao, C.Y. Li, Y.J. Zhang, et al., Adv. Mater. 30 (2018) 1804437.
[53] D.H. Zhao, X.Q. Yang, X.L. Hou, et al., J. Mater. Chem. B 7 (2019) 2484–2492.
[54] Y. Sun, C. Qu, H. Chen, et al., Chem. Sci. 7 (2016) 6203–6207.
[55] M.H. Wang, N.G. Chen, J. Biophotonics 12 (2019) e201800459.
[56] X. Li, M. Jiang, Y. Li, et al., Mater. Sci. Eng. 100 (2019) 260–268.
[57] Y. Miao, C. Gu, Y. Zhu, et al., ChemBioChem 19 (2018) 2522–2541.
[58] H. Wan, H.T. Du, F.F. Wang, H.J. Dai, Adv. Funct. Mater. 29 (2019) 1900566.
[59] N. Chen, Y. He, Y. Su, et al., Biomaterials 33 (2012) 1238–1244.
[60] L.V. Garmanchuk, M.N. Borovaya, A.O. Nehelia, et al., Cytol. Genet. 53 (2019) 132–142.
[61] Y. Xu, Z.W. Yang, J.B. Qiu, Z.G. Song, Mater. Express 8 (2018) 99–104.
[62] A. Badawi, Physica E 109 (2019) 107–113.
[63] Q.X. Wen, Y.J. Zhang, C.Y. Li, et al., Angew. Chem. Int. Ed. 58 (2019) 11001–11006.
[64] F.F. An, X.H. Zhang, Theranostics 7 (2017) 3667–3689.
[65] D.H. Zhao, J. Yang, R.X. Xia, et al., Chem. Commun. 54 (2018) 527–530.
[66] Y.N. Li, Y.T. Chang, X.F. Lian, et al., J. Biomed. Nanotechnol. 14 (2018) 1515–1542.
[67] J.C. Hsu, P.C. Naha, K.C. Lau, et al., Nanoscale 10 (2018) 17236–17248.
[68] H.D.A. Santos, E.C. Ximendes, M.D.C. Iglesias-de la Cruz, et al., Adv. Funct. Mater. 28 (2018) 1803924.
[69] S.I. Sadovnikov, A.I. Gusev, J. Mater. Chem. A 5 (2017) 17676–17704.
[70] B. del Rosal, B. Jia, D. Jaque, Adv. Funct. Mater. 28 (2018) 1803733.
[71] R.C. Sharma, Y.A. Chang, Bull. Alloy Phase Diagr. 7 (1986) 263–269.
[72] C. Wagner, J. Chem. Phys. 21 (1953) 1819–1827.
[73] X. Wang, N. Wang, L. Li, et al., RSC Adv. 7 (2017) 32536–32542.
[74] P. Jiang, Z.Q. Tian, C.N. Zhu, Z.L. Zhang, D.W. Pang, Dots Chem. Mater. 24 (2011) 3–5.
[75] V.A. Öberg, X. Zhang, M.B. Johansson, E.M.J. Johansson, Chem. Nano Mater. 4 (2018) 1223–1230.
[76] C. Zhang, S. Zhang, L. Yu, et al., Mater. Lett. 85 (2012) 77–80.
[77] W.P. Lim, Z. Zhang, H.Y. Low, W.S. Chin, Angew. Chem. Int. Ed. 43 (2004) 5685–5689.
[78] L. Lv, H. Wang, Mater. Lett. 121 (2014) 105–108.
[79] X. Hou, X. Zhang, W. Yang, Y. Liu, X. Zhai, Mater. Res. Bull. 47 (2012) 2579–2583.
[80] Y.L. Zhang, X.Y. Xie, M. Liang, et al., Nanotechnology 27 (2016) 225602.
[81] M. Liu, Z. Xu, B. Li, et al., Mater. Lett. 65 (2011) 555–558.
[82] H.J. Zhai, H.S. Wang, Mater. Res. Bull. 43 (2008) 2354–2360.
[83] Y. Zhao, D. Zhang, W. Shi, F. Wang, Mater. Lett. 61 (2007) 3232–3234.
[84] J. Kang, J. Yu, A. Li, et al., iScience 15 (2019) 119–126.
[85] S. Yan, H. Wang, Y. Zhang, S. Li, Z. Xiao, J. Non-Cryst. Solids 354 (2008) 5559–5562.
[86] D. Wang, C. Hao, W. Zheng, et al., Adv. Mater. 20 (2008) 2628–2632.

[87] M. Chen, L. Gao, Mater. Lett. 60 (2006) 1059–1062.
[88] Z. Zhuang, Q. Peng, X. Wang, Y. Li, Angew. Chem. Int. Ed. 46 (2007) 8174–8177.
[89] M. Karimipour, M. Bagheri, M. Molaei, J. Electron. Mater. 48 (2019) 2555–2562.
[90] L. Dong, G. Ji, Y. Liu, et al., Nanoscale 10 (2018) 825–831.
[91] X. Lai, X. Feng, J. Hu, et al., J. Nanopart. Res. 17 (2015) 113.
[92] P. Basyach, A. Choudhury, Mater. Res. Bull. 48 (2013) 2543–2548.
[93] Z. Sun, Z. Yang, J. Zhou, et al., Angew. Chem. Int. Ed. 48 (2009) 2881–2885.
[94] S. Xiong, B. Xi, K. Zhang, et al., Sci. Rep. 3 (2013) 2177.
[95] L. Motte, F. Billoudet, M.P. Pileni, J. Phys. Chem. 99 (1995) 16425–16429.
[96] M.C. Brelle, J.Z. Zhang, L. Nguyen, R.K. Mehra, J. Phys. Chem. A 103 (1999) 10194–10201.
[97] F. Gao, Q.Y. Lu, D.Y. Zhao, Nano Lett. 3 (2003) 85–88.
[98] Z. Liu, J. Liang, D. Xu, J. Lu, Y. Qian, Chem. Commun. (2004) 2724–2725.
[99] F. Hu, C. Li, Y. Zhang, et al., Nano Res. 8 (2015) 1637–1647.
[100] M.Y. Qin, X.Q. Yang, K. Wang, et al., Nanoscale 7 (2015) 19484–19492.
[101] H.D. Santos, D. Ruiz, G. Lifante, et al., Nanoscale 9 (2017) 2505–2513.
[102] G.S. Hong, J.T. Robinson, Y.J. Zhang, et al., Angew. Chem. Int. Ed. 51 (2012) 9818–9821.
[103] L. Ma, L. Li, J. Nanomater, Mol. Nanothechnol. 5 (2016) 1000182.
[104] N. Mukherjee, S. Jana, G. Gopal Khan, A. Mondal, J. Appl. Phys. 112 (2012) 124324.
[105] X. Wang, S. Zhang, Z. Zhang, Mater. Chem. Phys. 107 (2008) 9–12.
[106] J. Yang, J.Y. Ying, Chem. Commun. (2009) 3187–3189.
[107] D. Ayodhya, G. Veerabhadram, J. Photochem. Photobiol. B 157 (2016) 57–69.
[108] Z. Wang, Y. Ma, X. Yu, et al., Adv. Funct. Mater. 28 (2018) 1800732.
[109] J. Gao, C. Wu, D. Deng, P. Wu, C. Cai, Adv. Healthc. Mater. 5 (2016) 2437–2449.
[110] Y. Wang, X.P. Yan, Chem. Commun. 49 (2013) 3324–3326.
[111] J. Zhang, G. Hao, C. Yao, et al., ACS Appl. Mater. Interfaces 8 (2016) 16612–16621.
[112] H.Y. Yang, Y.W. Zhao, Z.Y. Zhang, H.M. Xiong, S.N. Yu, Nanotechnology 24 (2013)055706.
[113] L. Tan, A. Wan, H. Li, Langmuir 29 (2013) 15032–15042.
[114] X. Chen, L. Ding, P. Liu, Q. Wang, Surf. Interface Anal. 46 (2014) 301–306.
[115] R. Gui, J. Sun, D. Liu, Y. Wang, H. Jin, Dalton Trans. 43 (2014) 16690–16697.
[116] J.R. Wu, D.H. Bremner, S.W. Niu, et al., J. Biomed. Nanotechnol. 15 (2019) 1415–1431.
[117] J. Feng, Y. Li, Z. Gao, et al., Biosens. Bioelectron. 99 (2018) 14–20.
[118] X. Lu, L. Li, W. Zhang, C. Wang, Nanotechnology 16 (2005) 2233–2237.
[119] G. Hong, J.T. Robinson, Y. Zhang, et al., Angew. Chem. Int. Ed. 51 (2012) 9818–9821.
[120] T. Yang, Y. Tang, L. Liu, et al., ACS Nano 11 (2017) 1848–1857.
[121] Y.P. Du, B. Xu, T. Fu, et al., J. Am. Chem. Soc. 132 (2010) 1470–1471.
[122] A.K. Suresh, M.J. Doktycz, W. Wang, et al., Acta Biomater. 7 (2011) 4253–4258.
[123] J. Jang, K. Cho, S.H. Lee, S. Kim, Mater. Lett. 62 (2008) 1438–1440.
[124] J. Qiao, H. Zhang, G. Li, et al., Sep. Purif. Technol. 211 (2019) 843–856.
[125] H.I. Elsaeedy, Mater. Sci. Semicond. Process. Mater. Sci. Forum 93 (2019) 360–365.
[126] X.Z. Yuan, H.Q. Xu, Y. Shan, K.Z. Chen, Chem. Soc. Rev. 809–810 (2014) 39–42.
[127] Z. Zhuang, Q. Peng, Y. Li, Chem. Soc. Rev. 40 (2011) 5492–5513.
[128] L.P. Liu, Q. Peng, Y.D. Li, Inorg. Chem. 47 (2008) 5022–5028.
[129] J.H. Xiang, H.Q. Cao, Q.Z. Wu, et al., J. Phys. Chem. C 112 (2008) 3580–3584.
[130] I. Hocaoglu, M.N. Çizmeciyan, R. Erdem, et al., J. Mater. Chem. 22 (2012) 14674–14681.
[131] H. Zhang, B.R. Hyun, F.W. Wise, R.D. Robinson, Nano Lett. 12 (2012) 5856–5860.
[132] P. Jiang, C.N. Zhu, Z.L. Zhang, Z.Q. Tian, D.W. Pang, Biomaterials 33 (2012) 5130–5135.
[133] L. Dong, Y. Chu, Y. Liu, L. Li, J. Colloid Interface Sci. 317 (2008) 485–492.
[134] Y. Zhang, Y. Liu, C. Li, X. Chen, Q. Wang, J. Phys. Chem. C 118 (2014) 4918–4923.
[135] M. Shakouri-Arani, M. Salavati-Niasari, Spectrochim. Acta Part A 133 (2014) 463–471.
[136] X. Wang, W. Liu, J. Hao, X. Fu, B. Xu, Chem. Lett. 34 (2005) 1664–1665.
[137] L.V. Trandafilović, V. Djoković, N. Bibić, M.K. Georges, T. Radhakrishnan, Mater. Lett. 64 (2010) 1123–1126.
[138] H. Zhang, K. Li, Z. Ma, Colloids Surf. A 402 (2012) 94–101.
[139] L. Armelao, R. Bertoncello, E. Cattaruzza, et al., J. Mater. Chem. 12 (2002) 2401–2407.
[140] R. Ahmad, R. Srivastava, H. Bhardwaj, et al., ChemistrySelect 3 (2018) 5620–5629.
[141] B. Bezares, Y. Jana, L. Cottet, A. Castillo, Mater. Express 8 (2018) 450–456.
[142] S.U. Din, M. Hassan, S. Khalid, et al., Mater. Express 8 (2018) 85–92.
[143] F.D. Duman, I. Hocaoglu, D.G. Ozturk, et al., Nanoscale 7 (2015) 11352–11362.
[144] Q. Yang, J. Peng, K. Shi, et al., J. Control. Release 308 (2019) 29–43.
[145] J. Peng, Q. Yang, Y. Xiao, et al., Adv. Funct. Mater. 29 (2019) 1900004.
[146] Q. Yang, J. Peng, Y. Xiao, et al., ACS Appl. Mater. Interfaces 10 (2018) 150–164.
[147] X. Tang, L. Tan, K. Shi, et al., Acta Pharm. Sin. B 8 (2018) 587–601.
[148] X. Cai, X. Jia, W. Gao, et al., Adv. Funct. Mater. 25 (2015) 2520–2529.
[149] C. Tchounwou, S.S. Sinha, B.P. Viraka Nellore, et al., ACS Appl. Mater. Interfaces 7 (2015) 20649–20656.
[150] X. Song, H. Gong, S. Yin, et al., Adv. Funct. Mater. 24 (2014) 1194–1201.
[151] G. Wang, X. Wu, D. Cen, et al., J. Biomed. Nanotechnol. 14 (2018) 698–706.
[152] C. Li, X.Q. Yang, M.Z. Zhang, et al., Theranostics 8 (2018) 5662–5675.
[153] S. Kashida, Solid State Ionics 158 (2003) 167–175.
[154] A.I. Kryukov, A.L. Stroyuk, N.N. Zin'chuk, et al., J. Mol. Catal. A: Chem. 221 (2004) 209–221.
[155] Z. Xu, Y. Bando, W.L. Wang, X.D. Bai, D. Golberg, ACS Nano 10 (2016) 2982-2982.
[156] X. Zhang, M. Liu, H. Liu, S. Zhang, Biosens. Bioelectron. 56 (2014) 307–312.
[157] G.X. Zhu, Z. Xu, J. Am. Chem. Soc. 133 (2011) 148–157.
[158] L. Zhu, Z. Meng, G. Trisha, W.C. Oh, Chin. J. Catal. 33 (2012) 254–260.
[159] J. Liu, P. Raveendran, Z. Shervani, Y. Ikushima, Chem. Commun. (2004) 2582–2583.
[160] F. Lu, Y. Gong, W. Ju, et al., Inorg. Chem. Commun. 106 (2019) 233–239.
[161] S. Chand, E. Sharma, P. Sharma, J. Alloys Compd. 770 (2019) 1173–1180.
[162] D. Asik, M.B. Yagci, F. Demir Duman, H. Yagci Acar, J. Mater. Chem. B 4 (2016) 1941–1950.
[163] S.I. Sadovnikov, A.I. Gusev, Eur. J. Inorg. Chem. 2016 (2016) 4944–4957.
[164] S.I. Sadovnikov, A.I. Gusev, J. Mater. Chem. A 5 (2017) 17676–17704.
[165] D.H. Ortgies, Á.L. García-Villalón, M. Granado, et al., Nano Res. 12 (2019) 749–757.
[166] Q.B. Wang, Nanomed.-Nanotechnol. Biol. Med. 12 (2016) 464-464.
[167] L. Xing, S. Xu, J. Cui, L. Wang, J. Nanosci. Nanotechnol. 19 (2019) 4549–4555.
[168] D. Ozkan Vardar, S. Aydin, I. Hocaoglu, F.H. Yagci Acar, N. Basaran, Chem. Biol. Interact. 291 (2018) 212–219.
[169] J. Chen, T. Zhang, L. Feng, et al., Mater. Lett. 96 (2013) 224–227.
[170] C. Lu, G. Chen, B. Yu, H. Cong, Adv. Eng. Mater. 20 (2018) 1700940.
[171] M.L. Pang, J.Y. Hu, H.C. Zeng, J. Am. Chem. Soc. 132 (2010) 10771–10785.
[172] D. Ayodhya, G. Veerabhadram, J. Mol. Struct. 1186 (2019) 423–433.
[173] L.L. Guo, H. Chen, N.Y. He, Y. Deng, Chin. Chem. Lett. 29 (2018) 1829–1833.
[174] J. Sheng, L. Wang, Y. Han, et al., Small 14 (2018) 1702529.
[175] C.Y. Li, F. Li, Y.J. Zhang, et al., ACS Nano 9 (2015) 12255–12263.
[176] C. Levard, B.C. Reinsch, F.M. Michel, et al., Environ. Sci. Technol. 45 (2011) 5260–5266.
[177] G. Rotko, J. Cichos, E. Wysokinska, M. Karbowiak, W. Kalas, Colloids Surf. B Biointerfaces 181 (2019) 119–124.
[178] H. Chen, B. Li, M. Zhang, et al., Nanoscale 6 (2014) 12580–12590.
[179] F.D. Duman, M. Erkisa, R. Khodadust, et al., Nanomedicine 12 (2017) 2319–2333.
[180] C. Li, Y. Zhang, G. Chen, et al., Adv. Mater. 29 (2017) 1605754.
[181] C. Song, Y. Zhang, C. Li, et al., Adv. Funct. Mater. 26 (2016) 4192–4200.